Confined Normal-Shock/Turbulent-Boundary-Layer Interaction Followed by an Adverse Pressure Gradient

M. Sajben,* M. J. Morris,† T. J. Bogar,† and J. C. Kroutil‡
McDonnell Douglas Research Laboratories, St. Louis, Missouri 63166

A steady, nominally two-dimensional interaction of a normal shock with a turbulent boundary layer over a flat surface is investigated experimentally. The approach Mach number is 1.34 and the Reynolds number based on the momentum thickness of the approach boundary layer is 14,600. The boundary layer displays intermittent flow reversal (incipient detachment) at the foot of the shock. The experiment differs from similar past studies by the imposition of an extended adverse pressure gradient region downstream of the shock and by a relatively high ratio of approach boundary-layer thickness to channel height. The time-mean and fluctuating velocity fields were explored in detail using laser Doppler velocimetry. Spatial distributions of turbulence kinetic energy, shear stress, and turbulence production are presented.

Nomenclature

a = speed of sound
b = width of channel, 139.7 mm
C_f = skin-friction coefficient, based on u_e
H = δ^*/θ, shape factor
H_i = δ_i^*/θ_i, incompressible shape factor
h = channel height
k = $\frac{1}{2}(\hat{u}^2 + \hat{v}^2 + \hat{w}^2)$, turbulence kinetic energy
M = Mach number
P = rate of turbulence kinetic energy production
p = pressure
Re_θ = Reynolds number based on momentum thickness
U, V, W = time-mean velocity components in the x,y,z directions, normalized by a^*
u_τ = $\sqrt{(\tau_w/\rho_e)}$, friction velocity
u, v, w = time-mean velocity components in the x,y,z directions
x,y,z = Cartesian space coordinates, defined in Fig. 3
$\tilde{x}$ = $(x - x_0)/\delta_0^*$, normalized x coordinate
$\tilde{y}$ = y/δ_0^*, normalized y coordinate
γ_{pu} = fraction of time $(u + u')$ is negative
δ = full thickness of boundary layer, defined in text
δ^* = compressible displacement thickness, $\int_0^\delta [1-(\rho/\rho_e)^n(u/u_e)]\, dy$, with $n = 1$
δ_i^* = incompressible displacement thickness, $= \delta^*$ with $n = 0$
ν = kinematic viscosity
ρ = density
τ_w = wall shear stress
θ = compressible momentum thickness, $\int_0^\delta (\rho/\rho_e)^n(u/u_e)[1 - (u/u_e)]\, dy$, with $n = 1$
θ_i = incompressible momentum thickness, $= \theta$ with $n = 0$

Superscripts

$*$ = sonic condition (except for δ^*)
$'$ = fluctuating component
$\hat{}$ = root-mean-squared value of fluctuating component

Subscripts

e = at boundary-layer edge
i = incompressible
mx = maximum value (for a fixed x)
p = plenum chamber
t = total (stagnation) value
w = on wall
v = quantity associated with Van Driest-transformed velocity profile
0 = at $x = -44.5$ mm

Other

$\langle\rangle$ = time-averaged value

Introduction

TRANSONIC interactions between normal shocks and turbulent boundary layers are important in many high-speed aircraft and missile applications, especially in supersonic inlets

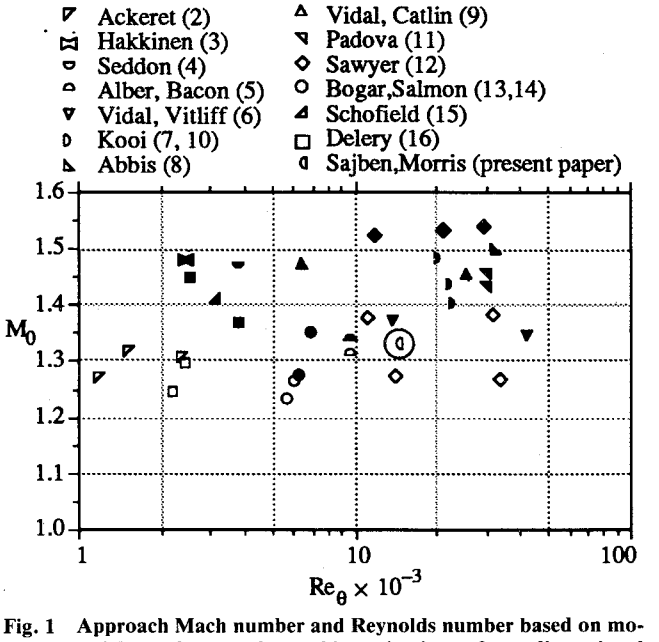

Fig. 1 Approach Mach number and Reynolds number based on momentum thickness for experimental investigations of two-dimensional transonic-shock/boundary-layer interactions. Open symbols indicate attached flows, full symbols denote shock-induced separation. References given parenthetically in the legend.

Received May 8, 1990; revision received Sept. 13, 1990; accepted for publication Sept. 28, 1990.

*McDonnell Douglas Fellow. Associate Fellow AIAA.
†Scientist. Member AIAA.
‡Section Chief, Laboratory. Member AIAA.

where the interaction exerts a dominant influence over the entire subsonic flowfield downstream of the shock. The function of an inlet is to capture flow and decelerate it to a moderate subsonic Mach number, with minimal losses. For this purpose, the terminal shocks in supersonic inlets are always followed by additional subsonic deceleration in a divergent section (diffuser). The additional deceleration may greatly modify the interactions compared to those occurring in constant-area channels, especially if the shock Mach number is high enough to cause shock-induced separation.

Numerous experimental and theoretical studies of normal-shock/boundary-layer-interaction (NSBLI) have been published.[1] A set of Mach and Reynolds number combinations over which nominally two-dimensional transonic interactions have been explored is illustrated in Fig. 1. Only flows with no transverse curvature and with no (or at most mild) streamwise curvature were included.[2-16] From this set of studies, only the work of Schofield[15] and the transonic diffuser experiments of Bogar[13] and Salmon[14] address NSBLIs coupled with a subsequent adverse pressure gradient.

The present study is an experimental investigation of a nominally two-dimensional, nominally steady interaction between a normal shock and a turbulent boundary layer on a flat surface in a rectangular-cross-section channel. Downstream of the shock the channel diverges, with a maximum divergence angle of five degrees to an overall area ratio of 1.305. The approach flow is uniform with a freestream Mach number of 1.34. The boundary layer is fully turbulent and the Reynolds number, based on the momentum thickness immediately before the shock, is 14,600. A spark schlieren photo of the flowfield is shown in Fig. 2.

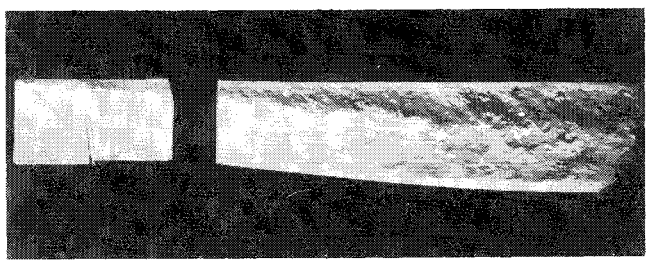

Fig. 2 Spark schlieren photograph of flowfield. Diagonal line starting at the left top corner is a weak Mach wave initiated by a butt joint on the top wall.

The ratio of the boundary-layer displacement thickness to the channel height (blockage) at the beginning of the interaction for this experiment is a relatively high 0.014. In comparison, the blockage in the majority of flows included in Fig. 1 is below 0.01. In operational inlets, blockage values vary widely with design and operating condition; values of 0.03 are common, and significantly higher values may occur.

Experimental Equipment and Procedures

Experimental Model

The experimental apparatus, diagnostic techniques, and data processing procedures are described in Ref. 17 and only a brief discussion is given in what follows.

The experimental model (Fig. 3) consists of a supersonic nozzle, an approach section of nearly constant area, a divergent test section, and a constant-area channel serving as a termination. The top wall, on which the interaction of interest occurs, forms a single planar surface from the nozzle exit to the exhaust. Coordinates of the bottom wall are given in Ref. 17.

The two-dimensional supersonic nozzle has two symmetric, contoured walls. The side-wall boundary layers are removed through side-wall slots at the nozzle exit ($x = -279.5$ mm). The bottom-wall boundary layer is removed through a suction slot at the location of the shock ($x = 0$). The total area of the three slots is 34% of the nozzle exit area. The leading edge of the bottom slot inner wall (point A in Fig. 3) serves as a shock holder to minimize shock oscillations. A new bottom-wall boundary layer is initiated at this location with essentially zero thickness. The final section of the model is a region where the streamwise derivatives of most flow properties are quite small, thereby establishing a downstream boundary condition that can be modeled well in theoretical descriptions. A hinged flap is mounted on the top wall at the downstream end of the model, permitting variation of the exit area. The flow is choked at this point, such that the flap creates a variable-size throat that can be used to control the shock position precisely.

Particular care was taken during the design of the present experiment to minimize three-dimensional effects. One effective design measure was the choice of the relatively high cross-section aspect ratio of $b/h = 2.9$. This value is significantly higher than the 1.2 value typical of most past experiments and is exceeded only by the experiments of Kooi[7] ($b/h = 3.4$) and by the diffuser experiments of Refs. 13, 14, 18, and 19 ($b/h = 3.6$–3.9).

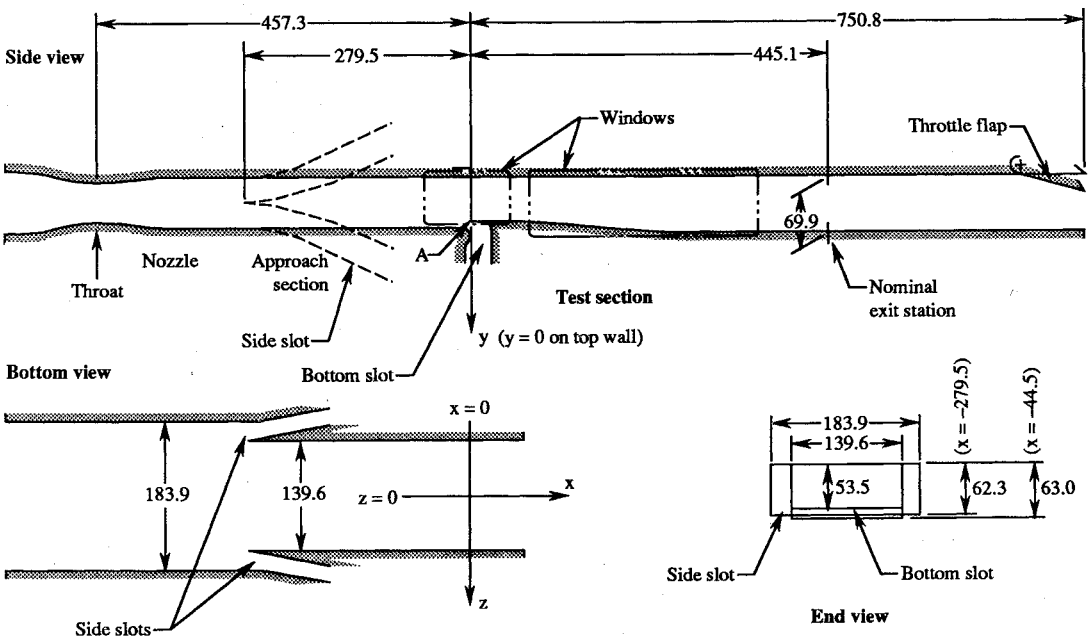

Fig. 3 Experimental apparatus for shock/boundary-layer interaction studies.

Additional measures designed into the experiment to minimize three-dimensional flow features are the removal of the side-wall and bottom-wall boundary layers through the respective slots. The streamwise lengths available for boundary-layer growth upstream of the shock are thus different on the various walls, the top wall being the longest. The result is that the top-wall boundary layer dominates the flow at the shock. The displacement area associated with the top wall is 63% of the total displacement area of all four walls. This fraction was obtained by calculation and verified by measurements; it is significantly greater than the 20–30% typical of most past experiments.

Filtered, dry air was supplied to the facility at a typical rate of 4.5 kg/s. The plenum chamber stagnation pressure was kept at 225 kPa ± 1% by a computer-operated digital control valve for all runs. Stagnation temperature was not controlled and varied according to weather conditions within the range 300 ± 15 K. The temperature variation resulted in corresponding slight variations of the unit Reynolds number and the speed of sound. The Reynolds number per unit length just upstream of the shock was 20.5 ± 1.4 × 10^6/m.

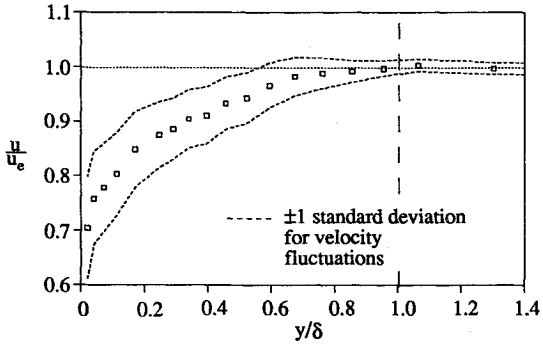

a) Mean-velocity profile, $U_{e0} = 1.263$, $\delta = 6.6$ mm

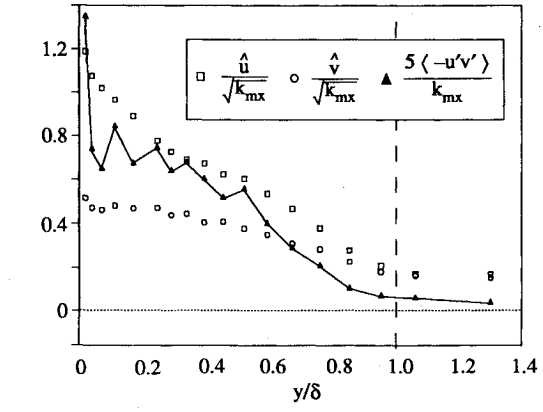

b) Turbulence intensities and (five times) the shear stress, $(k_{mx}/a_0^{*2}) = 1.021 \times 10^{-2}$

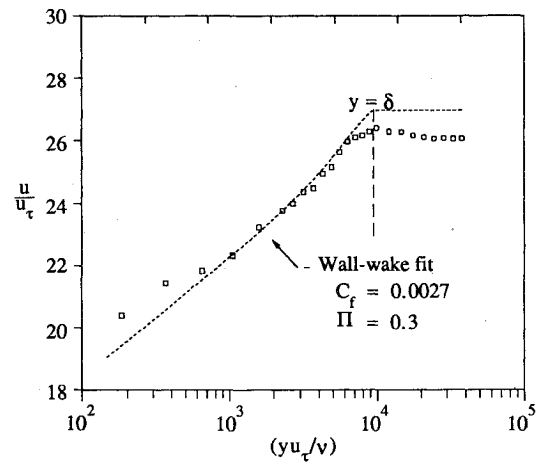

c) Clauser plot with best wall-wake fit

Fig. 4 Initial conditions at $x_0 = -44.5$ mm.

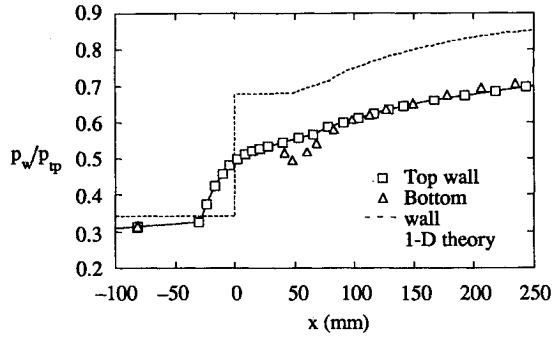

Fig. 5 Pressure distributions on the flat top wall and the curved bottom wall. The one-dimensional prediction based on geometric area variation and accounting for an $M = 1.34$ shock loss is also shown.

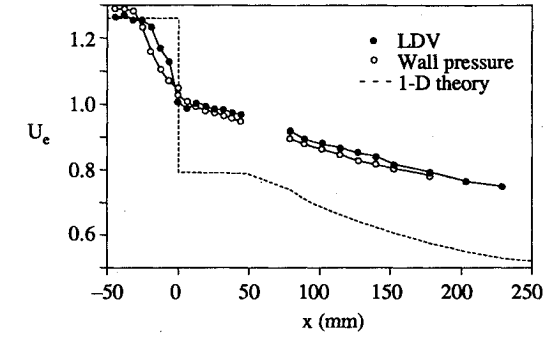

Fig. 6 Streamwise distributions of the velocity at the boundary-layer edge, as obtained by three different methods. Note small velocity "undershoot" at shock in the LDV data.

Diagnostic Methods

Numerous static-pressure taps were used to determine streamwise and spanwise wall-pressure distributions on the top, bottom, and side walls. High-speed schlieren, spark schlieren, and spark shadowgraph techniques were used to visualize the flow. Visual records were obtained by spark and high-speed photography and by videotaping the schlieren image. A mixture of lampblack and oil was used to determine the surface flow patterns on all four walls, representing the distribution of time-mean skin-friction directions.

The principal diagnostic tool was a laser-Doppler velocimeter (LDV) system that allowed the measurement of two coincident velocity components. The measurement volume had a diameter of 0.1 mm. Degradation of the signal-to-noise ratio prevented measurements closer than 0.2 mm of the wall. A Bragg cell was incorporated to produce a 40-MHz shift of the Doppler signal to remove velocity ambiguity. The scattered light was collected 25 deg off-axis in a forward scatter mode. The flow was seeded with submicrometer polydispersed particles of polyethylene glycol. This size range was sufficiently low to minimize the effects of particle dynamics. A more complete discussion of the LDV system can be found in Ref. 17.

Control of the pressure ratio implies that the Mach number distributions within the flow are the same for all runs. Since the speed of sound varied from run to run, the velocities measured by the LDV displayed a proportional run-to-run variation. To compensate for this variation, the measured velocities were normalized by the speed of sound at sonic condition.

Results and Discussion

Approach Condition and Two-Dimensionality

The first noticeable effects of the shock on the wall pressure and the boundary layer are observed just downstream of the

Table 1 Top-wall boundary-layer properties

x, mm	$\tilde{x}$	U_e	p_w/p_{tp}	δ, mm	δ^*, mm	θ, mm	H_i	$C_f \times 10^3$
− 44.5	0.0	1.263	0.3218	6.60	0.83	0.40	1.290	2.69
− 38.1	7.7	1.269	0.3234	6.53	0.75	0.36	1.297	2.80
− 31.8	15.3	1.254	0.3251	6.74	0.88	0.42	1.322	2.55
− 25.4	23.0	1.254	0.3592	7.36	0.97	0.46	1.330	2.55
− 19.0	30.6	1.232	0.4120	8.05	1.19	0.55	1.387	2.42
− 12.7	38.3	1.170	0.4499	11.03	1.92	0.87	1.501	1.95
− 6.3	46.0	1.125	0.4760	9.92	2.17	0.94	1.657	1.51
0.0	53.6	1.006	0.4936	8.12	2.57	1.03	1.929	0.70
6.3	61.2	0.986	0.5080	9.16	3.33	1.22	2.156	0.38
12.7	68.9	1.001	0.5184	10.68	3.64	1.33	2.142	0.40
19.0	76.5	0.994	0.5255	10.68	3.85	1.42	2.137	0.40
25.4	56.6	0.875	0.5324	10.61	3.89	1.42	2.172	0.38
31.8	91.8	0.983	0.5390	10.96	3.98	1.50	2.091	0.40
38.1	99.5	0.972	0.5444	11.79	4.00	1.54	2.061	0.45
44.5	107.1	0.969	0.5502	11.93	4.04	1.59	2.011	0.45
78.7	148.4	0.917	0.5886	15.63	4.64	2.00	1.877	0.59
88.9	160.7	0.895	0.5996	14.80	4.99	2.08	1.960	0.60
101.6	176.0	0.882	0.6100	16.46	5.57	2.27	2.023	0.50
114.3	191.3	0.867	0.6221	18.31	6.10	2.54	1.993	0.45
127.0	206.6	0.852	0.6341	19.69	6.62	2.76	2.008	0.45
139.7	221.9	0.841	0.6439	20.16	7.14	2.95	2.037	0.45
152.4	237.2	0.816	0.6524	21.54	7.20	3.06	2.000	0.45
177.8	267.8	0.792	0.6667	23.67	8.28	2.55	1.999	0.45
203.2	298.4	0.765	0.6789	27.17	9.96	4.38	1.967	0.40
228.6	329.0	0.748	0.6900	29.11	10.50	4.76	1.917	0.45

measurement station at $x = x_0 = -44.5$ mm. This location was chosen as the reference station reflecting the properties of the undisturbed approach flow. The mean-velocity profile and the most important turbulence quantities at this location are given in Figs. 4a and 4b. (In calculating k, the $\hat{w}$ contribution is assumed to be the arithmetic mean of $\hat{u}$ and $\hat{v}$.) The compressible displacement thickness is 0.83 mm, the compressible momentum thickness is 0.40 mm, and the incompressible shape factor is 1.29.

The reference velocity profile cannot be fitted well by the Coles wall-wake expression[20]; Fig. 4c illustrates the best fit we were able to obtain. The top-wall pressure data show evidence

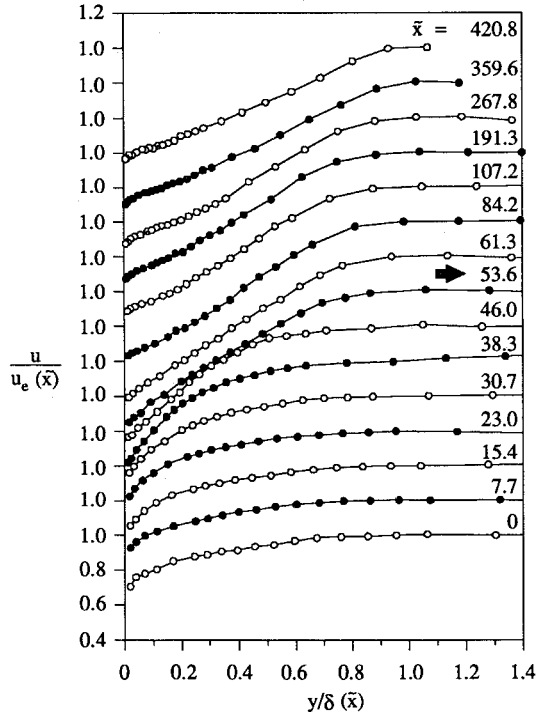

Fig. 7 Velocity profiles normalized by the local edge velocity and local thickness (both reference values are given in Table 1). Arrow indicates $\tilde{x}$ at shock holder.

that the flow in the approach section contained weak compression waves initiated by the vertical leading edges of the side-wall slots. The disturbances created by the glancing impingement of the compression waves on the boundary layer are probably responsible for the deviations from the wall-wake profile.

A natural transition to turbulence is believed to occur upstream of the nozzle throat. The installation of a single-element trip at the nozzle entrance ($x = -572$ mm) produced no measurable change in the mean profile of the boundary layer at $x = -88$ mm, as determined by a miniaturized pressure probe. The wall pressure distributions along the entire model were also unaffected by the trip.

Detailed velocity distributions were determined over three transverse cross sections, located before ($x = -38.1$ mm), shortly after ($x = 78.7$ mm), and well downstream ($x = 330.2$ mm) of the shock (Ref. 17 includes details). The data show that there always is a symmetric central region unaffected by the growth of the side-wall boundary layers. This effectively two-dimensional region occupies 90, 66, and 45% of the span at the three stations, respectively. We conclude that three-dimensional features are unimportant near the center plane, to at least $x = 300$ mm.

General Description of Flow

In Fig. 2, a fan of compression waves is observable upstream of the shock, induced by the initial thickening of the boundary layer. These waves tend to coalesce into a stronger wave, but do not form the distinct oblique shock and the lambda pattern characteristic of separated NSBLIs. Oil-flow traces showed no evidence of flow separation on either the top or the side walls. The markings indicated a slight thickening of corner flows at the shock, but the lines became parallel again after the shock. Information from additional sources, to be discussed later, confirms that boundary-layer detachment does not occur.

Past experience with similar flows in the same laboratory showed that incipient detachment invariably occurred at approach Mach numbers at or below 1.3.[13,14] Theoretical studies[21,22] also tend to indicate incipient separation at Mach numbers at or below 1.3. This conflict with expectations led to a thorough review of data available in the literature, and to Fig. 1 as a byproduct. This figure suggests that attached flow can

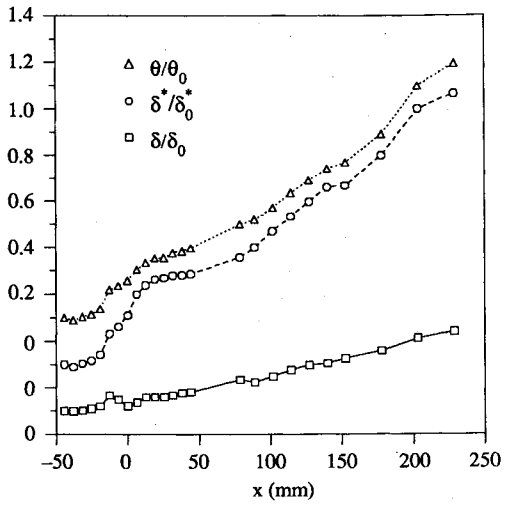

Fig. 8 Streamwise variation of compressible boundary-layer thicknesses, normalized by their respective values at $x_0 = -44.5$ mm, $\delta_0 = 6.6$ mm, $\theta_0 = 0.83$ mm, and $\delta_0^* = 0.40$ mm. Note vertical shifts of origin.

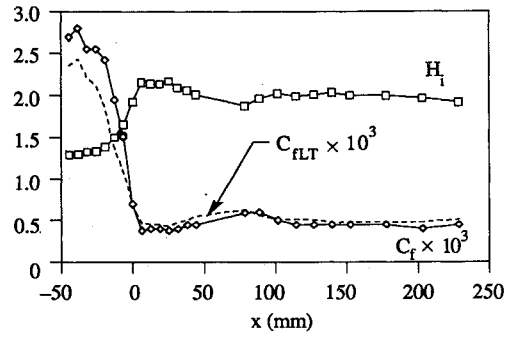

Fig. 9 Streamwise variation of the skin-friction coefficient C_f and the incompressible shape factor H_i. Skin-friction coefficient computed from the Ludwieg-Tillmann formula (C_{fLT}) is also shown.

occur at approach Mach numbers well above 1.3; in fact, attached flow has been reported at as high a value as 1.385.[12]

The bottom-wall boundary layer is thin, and has no significant effect on the interaction. The visible edges of the top and bottom boundary layers do not merge within the field of view, and there is a clearly defined core flow at the downstream end of the window.

High-speed schlieren movies (5000 frames/s) indicated that the shock displays a random jitter around its mean position. The bottom end of the shock is permanently attached to the shock holder, but the top end oscillates approximately ± 3 mm around the mean position. This shock oscillation is an inseparable feature of the flowfield. It has an adverse effect on LDV measurements near the shock by introducing a shock position error comparable to the shock motion amplitude and by creating uncertainties related to particle dynamics (particularly near the shock). The LDV system will intermittently detect preshock and postshock velocities, creating two peaks in the histogram. Such bimodal distributions yield unrealistically inflated rms values.

Time-Mean Data

The remainder of this paper will focus exclusively on data taken in the plane of symmetry ($z = 0$).

Figure 5 shows the streamwise distributions of static pressure on the top and bottom walls. The bottom-wall pressure distribution shows that the convex curvature near $x = 50$ mm causes a local reacceleration to slightly supersonic speed ($M = 1.07$), over an approximately 28-mm-long supersonic region. The region does affect the top-wall conditions slightly; there is a small, subsonic speed-up on the top wall at the same location, indicated by a small depression in the top-wall pressure distribution.

The top-wall pressure distribution is characterized by a very gradual change from supersonic to subsonic conditions. The interaction has a clear beginning, but no clear end; the shock-related pressure rise smoothly changes into the milder rise associated with the subsonic deceleration in the divergent channel. The supersonic interaction length (the distance from the beginning of the interaction to the location where the wall pressure is sonic) is almost twice that expected, $L/\delta_0^*/(H_i - 1) = 120$, instead of 70, as found by Delery[16] in his flows. Approximately half of the discrepancy is attributable to the broadening caused by shock oscillations.

An inviscid pressure distribution was computed from the channel area distribution, assuming a normal shock with $M = 1.34$ at $x = 0$ and using one-dimensional equations. The results, shown by a dashed line in Fig.5, indicate much higher pressures in the subsonic flow than those determined by measurement.

Figure 6 shows the streamwise distribution of the edge velocities obtained from LDV measurements. The edge velocities computed from measured data (wall static pressure, the plenum stagnation temperature, and the freestream total pressure) are also shown. For $x < 0$, p_{te} was assumed to be equal to the plenum static pressure. For $x > 0$, $p_{te} = 0.972\ p_{te}$ was taken, accounting for losses across a normal shock with $M = 1.34$. LDV and pressure-based velocities show good agreement in the subsonic region, but differ considerably at the shock. The differences are believed to be related to pressure gradients in the y direction.

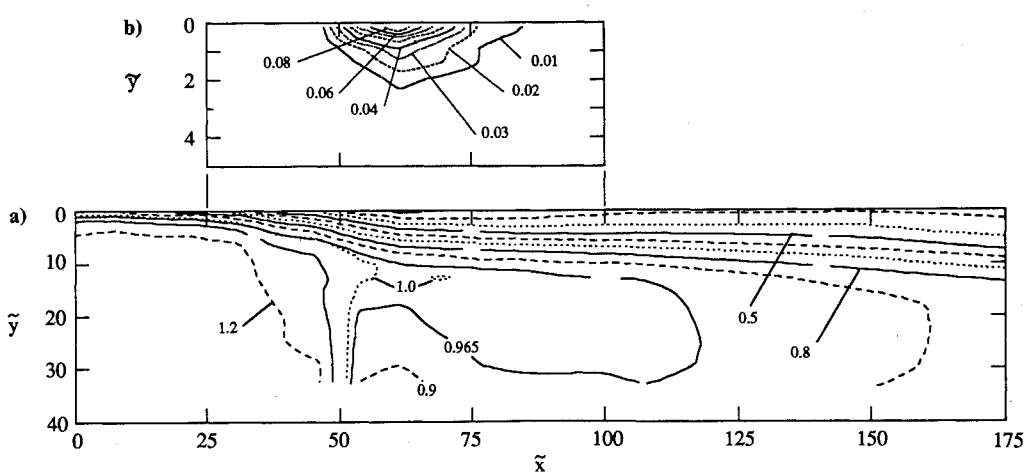

Fig. 10 Contours of a) U = constant, illustrating the abrupt thickening of the boundary layer at the shock; b) γ_{pu} = constant ($\tilde{x}$-scales identical, $\tilde{y}$-scale expanded on b).

The velocity distribution computed from the channel area distribution, using inviscid, one-dimensional theory, is also shown in Fig. 6: the prediction is much below the experimental results. The combination of high measured velocities and low measured pressures demonstrates the presence of large displacement effects in this flow. The postshock velocities are close to sonic; thus it is not surprising that even the minor area variations caused by displacement effects result in major changes of velocity and pressure.

Time-Mean Velocity Field

LDV data were obtained over a stretched, wall-conforming grid containing 25 streamwise stations and 20–25 points in the y direction. The edge of the boundary layer ($y = \delta$) was determined as the nearest location to the wall where the slope of the velocity profile became zero. At a number of locations a velocity maximum existed at the profile edge, allowing an unambiguous determination of δ. The determination became somewhat subjective when the freestream velocity was constant within the accuracy of the measurement.

The velocity profiles are presented in Fig. 7, normalized by local values of the boundary-layer thickness [$\delta(x)$] and by the edge velocity $u_e(x)$. The distributions of these local reference quantities are given numerically in Table 1. [Note that in this type of local normalization the previously used reference velocity (a^*) cancels $u/u_e = U/U_e$.] For easier comparison with earlier results,[1,16] the x location of the profiles in Fig. 7 is characterized by their distance from the initial station (at $x = x_0$), normalized by the initial displacement thickness.

No negative time-mean U values were detected anywhere, supporting the visual finding of attached flow. No supersonic region ("tongue") was found downstream of the shock. The absence was expected, since this feature generally appears at Mach numbers of 1.4 or greater. There is, however, a nearly sonic velocity peak at the edge of the boundary layer, just downstream of the shock. The overshoot is attributed to a displacement effect: the fluid has to flow around the bulge appearing in the displacement surface at the shock. This bulge acts as a bluff body to the outer flow. Flows around bluff bodies typically include a high-velocity region near the "shoulder" of the body. Supersonic tongues are probably higher-speed versions of such overshoots.

To analyze the boundary layer, the velocity data were Van Driest-transformed,[23,24] assuming an adiabatic wall and a recovery factor of 0.88. The data were then fitted to a Coles wall/wake profile to determine the (transformed) skin-friction coefficient C_{fv}. The skin-friction coefficient applicable to the compressible flow was then obtained by retransforming: $C_f = C_{fv}(u_{ev}/u_e)^2$. The compressible and incompressible displacement and momentum thicknesses were also determined.

The thickness distributions are illustrated in Fig. 8, the shape parameter and the skin-friction coefficient in Fig. 9. The most remarkable feature of the boundary-layer thickness distributions of Fig. 8 is the absence of drastic variations or changes of thickness in the vicinity of the shock. In classical, constant-area interactions, the displacement thickness may develop a sharp maximum, with a peak having 15–20 times the initial value.[15] In the present flow δ^* and θ grow monotonically, although the growth rate at the shock is much higher than elsewhere.

As illustrated in Fig. 9, the shape factor H_i remains well below the separation value of 2.7, consistent with the attached character of the flow. The skin-friction coefficient (Fig. 9) drops sharply at the shock, and remains at a low, nearly constant level in the subsonic region. It never becomes zero, consistent with other indications of attached flow. The measured values are in good agreement with values calculated from the measured Re_θ and H_i, using the Ludwieg-Tillmann skin-friction formula.[25]

Figure 10a is a composite contour plot of the horizontal velocity component. The rapid thickening of the boundary layer at the shock is evident, as is the presence of the high-velocity overshoot region.

Table 2 Turbulence properties

$\tilde{x}$	$\tilde{y}_{kmx}$	$\left(\frac{k_{mx}}{a^{*2}}\right)\times 10^2$	$\tilde{y}_{uvmx}$	$\frac{\langle -u'v'\rangle_{mx}}{a^{*2}}\times 10^3$
0.0	0.31	1.021	1.30	1.477
7.7	0.31	1.107	0.31	2.347
15.3	0.31	1.461	0.31	3.145
23.0	0.31	1.485	0.31	3.426
30.6	0.67	1.794	0.81	3.946
38.3	0.97	2.385	1.69	4.221
45.9	2.12	2.759	2.03	3.862
53.6	1.67	2.769	1.26	3.856
61.2	3.08	2.738	2.15	4.040
68.9	3.44	2.670	2.28	4.692
76.5	4.82	2.446	3.56	4.896
84.0	5.47	2.448	3.56	5.161
91.8	5.25	2.305	3.60	5.577
99.5	5.78	2.259	4.36	5.713
107.1	6.03	2.209	5.43	5.722
148.4	8.39	2.097	6.06	5.061
160.7	7.64	2.138	7.30	5.530
176.0	9.46	2.101	7.83	5.061
191.3	9.92	2.136	8.46	4.934
206.6	10.77	2.095	10.20	4.897
221.9	11.45	2.068	8.52	4.753
237.2	10.25	1.862	9.14	4.535
267.8	13.45	1.786	12.44	4.701
298.4	16.36	1.451	17.28	3.690
329.0	17.21	1.396	18.06	3.651

Figure 10b illustrates the fraction of time the u velocity component is negative (γ_{pu}), in the form of a contour plot. Such reversal occurs only in a small region (note greatly enlarged scales), slightly downstream of the shock. The largest measured γ_{pu} value is 0.08, occurring very close to the wall. Using commonly accepted definitions for the characterization of the detachment process,[26] this degree of reversal is termed incipient detachment.

Turbulence Structure

The LDV measurements yield instantaneous velocities, which allow the calculation of the rms values and the time-mean value of the product of the two velocity components. In a compressible flow the Reynolds stresses involve the mean

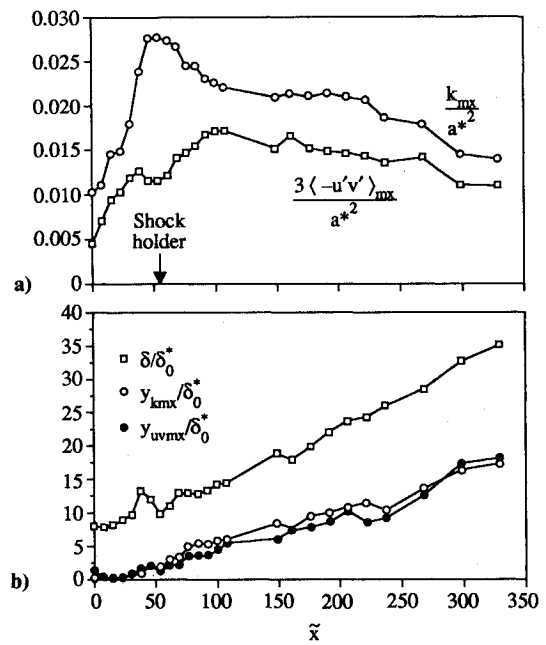

Fig. 11 Distributions of maximum turbulence kinetic energy and maximum shear stress: a) magnitudes, b) locations where the maxima occur. (The boundary-layer thickness δ is also shown for reference.)

and fluctuating densities at the same locations. However, density information is not available, and the exploration of the turbulence structure is limited to fluctuations of the velocity field only. Densities will be omitted and the quantity $\langle -u'v' \rangle$ will be referred to as the shear stress. This approximation amounts to applying the concepts of incompressible turbulence to the present flow.

The data will be normalized by x-dependent reference quantities (Table 2). The reference quantity chosen to normalize the turbulence properties is the maximum turbulence kinetic energy (k_{mx}) at the streamwise location of interest. The reference length for the y coordinate is the local boundary-layer thickness, $\delta(x)$.

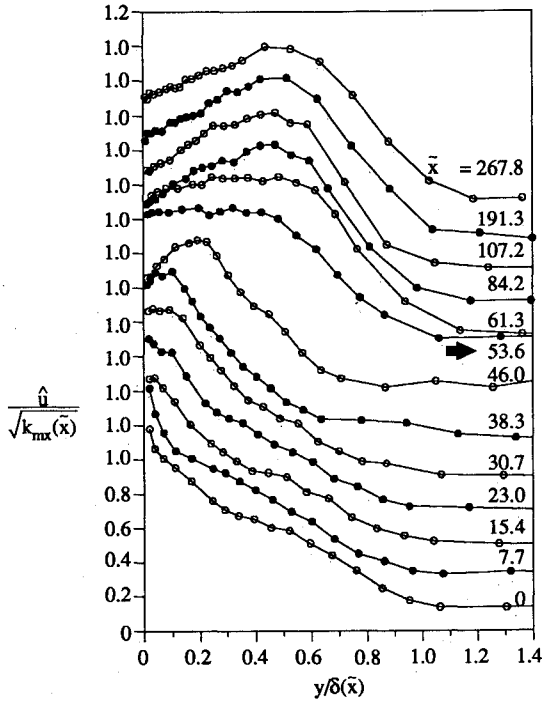

Fig. 12 Profiles of the rms value of the fluctuating u component, normalized by the square root of the local maximum turbulence kinetic energy (Table 2) and the local boundary-layer thickness (Table 1). Arrow indicates $\tilde{x}$ at shock holder.

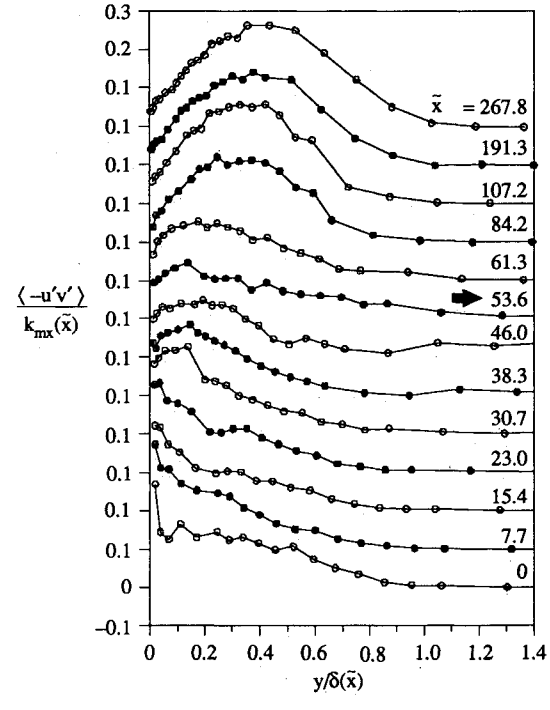

Fig. 13 Shear-stress profiles, normalized by the local maximum turbulence kinetic energy (Table 2) and the local boundary-layer thickness (Table 1). Arrow indicates $\tilde{x}$ at shock holder.

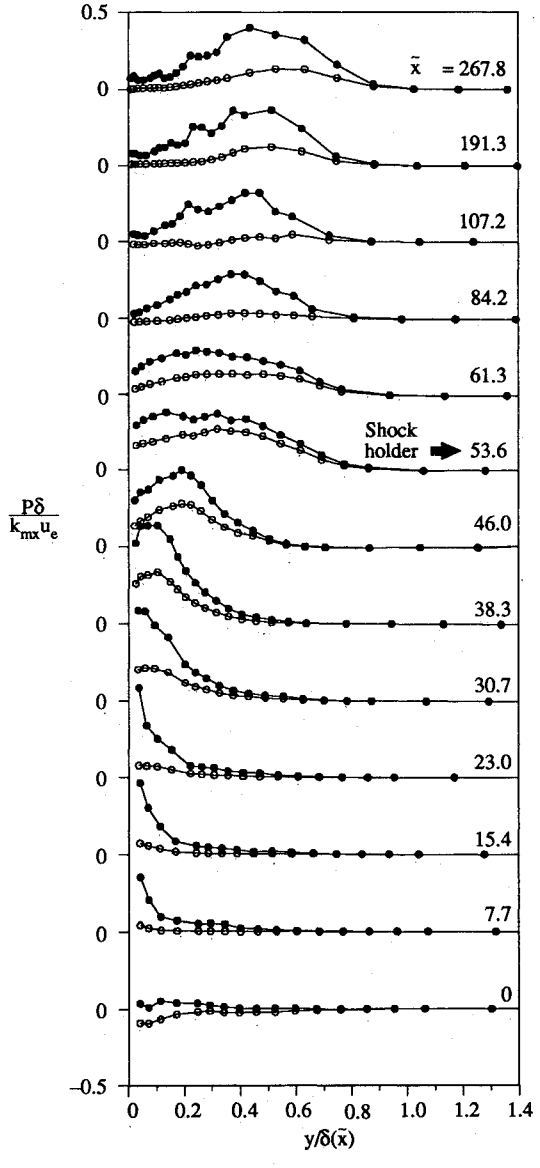

Fig. 14 Rates of turbulence kinetic-energy production. Open symbols represent contribution from normal stresses. Solid symbols describe total production, including contribution from shear stresses. All reference quantities are local, given in Tables 1 and 2.

Figure 11a shows the streamwise variation of k_{mx}, and the maximum values of the shear stress, $\langle -u'v' \rangle_{mx}$. The maximum turbulence kinetic energy reaches a peak value as a function of x very close to the shock. This peak coincides with the range of bimodal LDV histograms, and reflects the large velocity fluctuations obtained by intermittently detecting preshock and postshock velocities. A much flatter peak occurs in the maximum shear stress, approximately 50 displacement thicknesses further downstream. Similar features, including the sharp k_{mx} peak, are present in other data sets.[16] Note, however, that the magnitude of the fluctuations in the present experiment is approximately one-third of those reported in Ref. 16. The cause of this difference is not certain. The measurements were made in different facilities and with different instrumentation. The present flow was incipiently separated. Increasing the Mach number only slightly could result in a significant increase in the turbulence kinetic energy levels. Any or all of these factors could contribute to the difference.

The loci of the maxima are shown in Fig. 11b, along with the boundary-layer thickness δ for reference. The loci of the two types of maxima are virtually coincident. Initially the

maxima occur very close to the wall, but they gradually migrate outwards until, at $\tilde{x} = 300$, the maxima occur roughly in the middle of the boundary layer.

Figure 12 illustrates the $\hat{u}$ profiles at a number of $\tilde{x}$-locations. The outward migration of the maximum fluctuation level is evident. The fluctuation intensity shows locally high values at the shock (near $\tilde{x} = 53.6$), both near the wall and near the edge of the boundary layer. These regions of high apparent intensity probably reflect the LDV measurement problems caused by shock oscillations.

Figure 13 shows shear-stress profiles for a set of streamwise locations. The profiles do not display the high intensities at the shock and near the wall, as found in the $\hat{u}$ profiles. The absence of the local peaks is consistent with the notion that the shock oscillations are not associated with fluctuations of the v velocity component; there is no u-v correlation and thus the u fluctuations associated with shock oscillation do not contribute directly to the shear stress.

In incompressible flow, the turbulence production term in the turbulent kinetic energy equation is given, approximately, by

$$P = \langle -u'v' \rangle \frac{\partial u}{\partial y} - (\hat{u}^2 - \hat{v}^2)\frac{\partial u}{\partial x} \qquad (1)$$

where the two terms describe the shear-stress and normal-stress contributions, respectively. The time-mean data were smoothed by a cubic spline method—first in the y, then in the x direction—and the derivatives were determined from the computed coefficients of the polynomial fits. The turbulence quantities were not smoothed. The results are given in Fig. 14, illustrating both the total production and the contribution associated with the normal stresses alone.

The results show that the contribution of the normal stresses to the production of turbulence is comparable to the shear-stress contribution in the vicinity of the shock. Some of the normal-stress contributions are traceable to the high $\hat{u}$ values resulting from the shock oscillation problem. The y-distribution of the normal-stress contribution is similar to that of the total production. The peak production rates occur near the locations of maximum shear.

Summary and Conclusions

The interaction of an $M = 1.34$ normal shock with a turbulent boundary layer on a flat surface was explored experimentally. The shock was followed by an adverse pressure gradient, created by a diverging diffuser section. The ratio of the boundary-layer displacement thickness to the channel height was 0.014, significantly higher than the values used in most reported NSBLI experiments. The flow was essentially steady and three-dimensional effects were negligible. The flow was found to be in a state of incipient detachment, experiencing instantaneous backflow, at most 8% of the time. The flow is a borderline case in terms of several parameters: it is on the verge of separation, it has a high (although not excessive) blockage, and it contains a significant (but not severe) adverse pressure gradient downstream of the shock.

The flow properties at the edge of the boundary layer show a smooth merging of the shock and the subsequent subsonic deceleration. The integral thicknesses increase monotonically, in contrast to interactions taking place in constant-area channels, which tend to display large peaks in the displacement-thickness distributions.

The displacement effects are drastic, resulting in high, near-sonic velocities and correspondingly low static pressures in the subsonic flow. The reduced static pressure rise across the shock results in moderate pressure gradients that are probably responsible for the absence of separation at this relatively high-approach Mach number. Since these effects are all traceable to the large initial blockage, the results suggest that increasing blockage might tend to suppress separation for a given initial Mach number.

The turbulence structure is qualitatively similar to results obtained in constant-area channels by other investigators, although the intensity levels are lower by nearly a factor of three. The turbulence production is most intense in the immediate vicinity of the shock. The normal stresses contribute significantly to the production of turbulence kinetic energy in a region of ± 20 initial displacement thicknesses from the shock.

Acknowledgments

This research was conducted under the McDonnell Douglas Independent Research and Development Program. The authors thank Natalie L. Vignati and Ron Holtz for the design/construction/maintenance of much specialized instrumentation and equipment, and George T. Harmon and Ronald E. Price for operating a complex laboratory computer system. We also express our appreciation to co-op students who worked on this program: Richard W. Hoffman, Jeff L. Herrin, and Cory D. Martin provided able and often imaginative assistance in running the tests and processing the data.

References

[1]Delery, J., and Marvin, J. G., (ed.) "Shock-Wave Boundary Layer Interactions," AGARD Rept. AG-280, Feb. 1986.

[2]Ackeret, J., Feldman, F., and Rott, N., "Investigations of Compression Shocks and Boundary Layers in Gases Moving at High Speed," NACA TM 1113, Jan. 1947.

[3]Hakkinen, R. J., "Measurement of Skin Friction in Turbulent Boundary Layers at Transonic Speeds," Ph.D. Dissertation, Firestone Flight Sciences Lab., California Inst. of Technology, Pasadena, CA, 1954.

[4]Seddon, J., "The Flow Produced by Interaction of a Turbulent Boundary Layer with a Normal Shock Wave of Strength Sufficient to Cause Separation," Aeronautical Research Council, R&M 3502, March 1960.

[5]Alber, E. E., Bacon, J. W., Masson, B. S., and Collins, D. J., "An Experimental Investigation of Turbulent Transonic Viscous-Inviscid Interactions," AIAA Paper 71-565, 1971; also, *AIAA Journal*, Vol. 11, No. 5, 1973, pp. 620–627.

[6]Vidal, R. J., Witliff, P. A., Catlin, P. A., and Sheen, B. H., "Reynolds Number Effects on the Shock Wave—Turbulent Boundary Interactions at Transonic Speeds," AIAA Paper 73-661, July 1973.

[7]Kooi, J. W., "Experiment on Transonic Shock-Wave Boundary Layer Interaction," *Flow Separation*, AGARD Conference Proceedings, CP-168, 1975, pp. 30-1 to 30-10.

[8]Abbiss, J. B., East, L. F., Nash, C. R., Parker, P., Pike, E. R., and Sawyer, W. G., "A Study of the Interaction of a Normal Shock Wave and a Turbulent Boundary Layer Using a Laser Anemometer," Royal Aircraft Establishment Rept. TR-75141, Feb. 1976.

[9]Vidal, R. J., and Catlin, P. A., "Investigations of Shock Wave-Turbulent Boundary Layer Interactions at Transonic Speeds," Calspan Rept. WF-5746-A-1, Buffalo, NY, April 1977.

[10]Kooi, J. W., "Influence of Free-Stream Mach Number on Transonic Shock-Wave Boundary-Layer Interactions," National Aerospace Lab., Rept. NLR MP 78013 U, The Netherlands, May 1978.

[11]Padova, C., and Witliff, C. E., "The Effects of Wall-to-Total Temperature Ration on Shock Wave—Turbulent Boundary Layer Interactions at Transonic Speeds," Calspan Rept. WF-6091-A-1, Buffalo, NY, Oct. 1979.

[12]Sawyer, W. G., and Long, C. J., "A Study of Normal Shock-Wave Turbulent Boundary-Layer Interactions at Mach Numbers of 1.3, 1.4 and 1.5," Royal Aircraft Establishment Rept. TR 82099, Oct. 1982.

[13]Bogar, T. J., Sajben, M., and Kroutil, J. C., "Characteristic Frequencies of Transonic Diffuser Flow Oscillations," *AIAA Journal*, Vol. 21, No. 9, 1983, pp. 1232–1240.

[14]Salmon, J. T., Bogar, T. J., and Sajben, M., "Laser Doppler Measurements in Unsteady, Separated, Transonic Diffuser Flow," *AIAA Journal*, Vol. 21, No. 12, 1983, pp. 1690–1697.

[15]Schofield, W. H., "Interaction of a Turbulent Boundary Layer with a Normal Shock Wave Followed by an Adverse Pressure Gradient," Aeronautical Research Lab., Rept. AR-002-950, Melbourne, Victoria, Australia, April 1983.

[16]Delery, J., "Investigation of Strong Shock Turbulent Boundary Layer Interaction in 2-D Transonic Flows with Emphasis on Turbulence Phenomena," AIAA Paper 81-1245, June 1981; also, *AIAA Journal*, Vol. 21, No. 2, 1983, pp. 180–185.

[17]Sajben, M., Morris, M. J., Bogar, T. J., and Kroutil, J. C., "Confined Normal-Shock/Turbulent-Boundary-Layer Interaction

Followed by an Adverse Pressure Gradient," AIAA Paper 89-0354, Jan. 1989.

[18]Sajben, M., and Kroutil, J. C., "Effects of Initial Boundary Layer Thickness on Transonic Diffuser Flows," *AIAA Journal,* Vol. 19, No. 11, 1981, pp. 1386–1393.

[19]Sajben, M., Bogar, T. J., and Kroutil, J. C., "Experimental Study of Flows in a Two-Dimensional Inlet Model," *Journal of Propulsion and Power,* Vol. 1, No. 2, 1985, pp. 109–117.

[20]Coles, D., "The Law of the Wake in the Turbulent Boundary Layer," *Journal of Fluid Mechanics,* Vol. 1, July 1956, pp. 191–226.

[21]Inger, G. R., "Analysis of Transonic Normal Shock-Boundary Layer Interaction and Comparisons with Experiment," Virginia Polytechnic Inst. and State Univ., Rept. VPI-Aero-053, Blacksburg, VA, 1976.

[22]Melnik, R. E., and Grossman, B., "Further Developments in an Analysis of the Interaction of a Weak Normal Shock Wave with a Turbulent Boundary Layer," Grumman Res. Dept. RE-511J, Nov. 1975.

[23]Van Driest, E. R., "Turbulent Boundary Layer in Compressible Fluids," *Journal of the Aeronautical Sciences,* Vol. 18, No. 3, 1951, pp. 145–160.

[24]Cebeci, T., and Smith, A. M. O., *Analysis of Turbulent Boundary Layers,* Academic, New York, 1974, pp. 145–147.

[25]Schlichting, H., *Boundary Layer Theory,* fourth ed., McGraw-Hill, 1960, p. 575.

[26]Kline, S. J., Bardina, J. G., and Strawn, R. C., "Correlation of the Detachment of Two-Dimensional Turbulent Boundary Layers," *AIAA Journal,* Vol. 21, No. 1, 1983, pp. 68–73.